Draft version August 27, 2021
Typeset using LaTeX default style in AASTeX63

The 3D Galactocentric velocities of Kepler stars: marginalizing over missing RVs

Ruth Angus,[1,2,3] Adrian M. Price-Whelan,[2] Daniel Foreman-Mackey,[2] Joel Zinn,[4] Megan Bedell,[2] and Yuxi (Lucy) Lu[3,1]

[1]*Department of Astrophysics, American Museum of Natural History, 200 Central Park West, Manhattan, NY, USA*
[2]*Center for Computational Astrophysics, Flatiron Institute, 162 5th Avenue, Manhattan, NY, USA*
[3]*Department of Astronomy, Pupin Hall, Columbia University, Manhattan, NY, USA*
[4]*NSF Astronomy and Astrophysics Postdoctoral Fellow, Department of Astrophysics, American Museum of Natural History, 200 Central Park West, Manhattan, NY, USA*

ABSTRACT

Precise Gaia measurements of positions, parallaxes, and proper motions provide an opportunity to calculate 3D positions and 2D velocities (*i.e.* 5D phase-space) of Milky Way stars. Where available, spectroscopic radial velocity (RV) measurements provide full 6D phase-space information. Gaia will provide RVs for stars as faint as the 15th magnitude in its third data release, however there are now and will remain many stars without RV measurements. Without an RV it is not possible to directly calculate 3D stellar velocities, however it is still possible to *infer* 3D stellar velocities by marginalizing over the missing RV dimension. In this paper, we infer the 3D velocities of stars in the Kepler field in Cartesian Galactocentric coordinates ($v_{\mathbf{x}}$, $v_{\mathbf{y}}$, $v_{\mathbf{z}}$). We directly calculate velocities for around a third of all Kepler targets, using RV measurements available from the Gaia, LAMOST and APOGEE spectroscopic surveys. Using the velocity distributions of these stars as our prior, we infer velocities for the remaining two-thirds of the sample by marginalizing over the RV dimension. The median uncertainties on our inferred $v_{\mathbf{x}}$, $v_{\mathbf{y}}$, and $v_{\mathbf{z}}$ velocities are around 5, 18, and 4 kms^{-1}, respectively. We provide 3D velocities for a total of 150,278 stars in the Kepler field. These 3D velocities will enable kinematic age-dating, Milky Way stellar population studies, and many other scientific studies using the benchmark sample of well-studied Kepler stars. Although the methodology used here is broadly applicable to targets across the sky, our prior is specifically constructed from and for the Kepler field. Care should be taken to use a suitable prior when extending this method to other parts of the Galaxy.

Keywords: Milky Way Dynamics

1. INTRODUCTION

Gaia has revolutionized the field of Galactic dynamics by providing positions, parallaxes and proper motions with unparalleled precision, for a large number of Milky Way stars. So far, Gaia has provided positions, parallaxes and proper motions for around 1.7 billion stars, and radial velocities (RVs) for more than 7 million stars across its 1st, 2nd and early-3rd data releases (Gaia Collaboration et al. 2016, 2018, 2020). In combination, proper motion, position, and RV measurements provide full 6D phase-space information for any given star, which can be used to calculate its Galactic orbit. The orbits of stars are useful for kinematic age-dating, for exploring the secular dynamical evolution of the Galaxy, for differentiating between nascent and accreted stellar populations in the Milky Way's halo, and many other applications.

One particular motivation is to use Galactic kinematics to study stellar evolution, either by using vertical velocity dispersion as an age proxy, or by calculating stellar ages via an age-velocity dispersion relation (*e.g.* Angus et al. 2020; Lu et al. 2021). The ages of stars, particularly GKM stars on the main sequence, are difficult to measure because their luminosities and temperatures evolve slowly (see Soderblom 2010, for a review of stellar ages). Galactic kinematics provides an alternative, statistical dating method.

Older populations of stars are observed to have larger velocity dispersions than younger populations, and this is generally thought to be caused by dynamical heating of the Galactic disc by giant molecular clouds and spiral arms (*e.g.* Strömberg 1946; Wielen 1977; Nordström et al. 2004; Holmberg et al. 2007, 2009; Aumer & Binney 2009; Casagrande et al. 2011; Yu & Liu 2018; Ting & Rix 2019). This behavior is codified by empirically-calibrated Age-Velocity

dispersion Relations (AVRs), which typically express the relationship between age and velocity dispersion as a power law: $\sigma_v \propto t^{\beta}$, with free parameter, β (*e.g.* Holmberg et al. 2009; Yu & Liu 2018; Mackereth et al. 2019). These expressions can be used to calculate the ages of stellar populations from their velocity dispersions. However, AVRs are usually calibrated in 3D Galactocentric velocities, and most commonly in vertical velocity: $v_{\mathbf{z}}$ or W. Regardless of the coordinate system, some transformation from RV and proper motion in equatorial coordinates is usually required to calculate the kinematic ages of stars using an AVR.

RV measurements, combined with positions, parallaxes, and proper motions measured in the plane of the sky, complete the full set of information needed to calculate 3D stellar velocities. However, RV can generally[1] only be measured from a stellar spectrum – an observation that requires a significant number of photons and is thus expensive to obtain, particularly for faint stars. Fortunately however, the bulk circular velocity of the Galactic disc allows stellar velocities to be inferred by using an informative prior that is constructed from the velocities of stars with full 6D phase-space information. This will often result in a velocity that is not equally well-constrained in every direction, *i.e.* the probability density function of a star's velocity will be an oblate spheroid in 3D. In the equatorial coordinate system, a star's velocity will be tightly constrained in the directions of RA and dec, and only constrained by the prior in the radial direction. Transforming to any other coordinate system, a star's velocity probability density function will change shape via a transformation that depends on its position.

In this work, we provide 3D velocities in $v_{\mathbf{x}}$, $v_{\mathbf{y}}$, and $v_{\mathbf{z}}$ for Kepler targets. Our motivation is chiefly to calculate vertical velocities ($v_{\mathbf{z}}$) which can then be used to calculate the ages of stellar populations via an AVR, from which other empirical age-dating methods can be calibrated. For example, empirical or semi-empirical models that relate the magnetic activity or rotation periods of stars to their age can be used to infer the ages of some low-mass dwarfs (*e.g.* Skumanich 1972; Barnes 2003, 2007; Mamajek & Hillenbrand 2008; Matt et al. 2012; Angus et al. 2019; Claytor et al. 2020), however, these empirical relations are often poorly calibrated for low-mass and old stars (*e.g.* Angus et al. 2015; van Saders et al. 2016, 2018; Metcalfe & Egeland 2019; Curtis et al. 2020; Spada & Lanzafame 2019; Angus et al. 2020). In Angus et al. (2020) we used the velocities of Kepler stars in the direction of Galactic latitude, $v_{\mathbf{b}}$ as a proxy for vertical velocity. $v_{\mathbf{b}}$ can be calculated without an RV and it is similar to $v_{\mathbf{z}}$ for many Kepler stars because the Kepler field lies at low Galactic latitude. We used the $v_{\mathbf{b}}$ velocity dispersions of stars as an age proxy to explore the evolution of stellar rotation rates. In Lu et al. (2021) we used *vertical* velocity dispersion ($v_{\mathbf{z}}$) to calculate kinematic ages for Kepler stars with measured rotation periods using an age-velocity dispersion relation (AVR). Those vertical velocities were inferred by marginalizing over missing RVs using the method we describe in this paper. To expand upon that work and provide an opportunity to apply kinematic age-dating to more stars, we here calculate the 3D velocities of *all* Kepler targets. Although we focus on the Kepler field, the methodology presented in this paper is applicable to stars across the sky if a suitable prior is used.

There are several other applications for which the 3D velocity of a star is useful, even if its velocity is not equally well-constrained in every direction. For example, Oh et al. (2017) used Gaia proper motions to identify comoving pairs and groups of stars by marginalizing over missing RVs. In their study, the relative space motions of pairs of stars were used to establish whether they qualified as 'comoving'. In a pathological case where two stars (nearby on the sky) have near identical proper motions and completely different RVs, their method would incorrectly flag them as comoving stars, however in general the Gaia proper motion precision is sufficiently high to make these cases rare.

Another work that predicts 3D velocities of Gaia targets is Dropulic et al. (2021), in which the velocities of mock Gaia stars are predicted with a neural network. The network is trained on the velocities of stars *with* RVs and used to predict the velocities of stars without. The method we present here seeks to solve the same problem via a different methodology: we use Bayesian inference instead of a neural network. It is difficult to draw a direct comparison between their method and ours because we use different coordinate systems (we use Cartesian, and they use cylindrical coordinates), and because we focus on different populations – they predict velocities for the entire Gaia catalog, whereas we concentrate on a small part of the sky. The two approaches will be useful for different scientific applications, and it is extremely useful to have multiple approaches to solving this fundamental problem in astronomy.

This paper is laid out as follows. In section 2 we describe the data used in this paper. In section 3 we describe how we calculate the kinematic ages of Kepler stars from their positions, proper motions and parallaxes, marginalizing over missing RVs. We also justify the choice of prior probability density function (PDF). In section 4 we present the 3D velocities of 150,278 Kepler stars and explore the accuracy and precision of our method.

[1] RVs can also be derived from perspective acceleration for high proper motion stars (*e.g.* Lindegren & Dravins 2021).

2. THE DATA

We used the Kepler-Gaia cross-matched catalog available at gaia-kepler.fun, which contains 198,451 Kepler targets, cross-matched with Gaia targets within in a 1" radius. This catalog includes positions, parallaxes, and proper motions from Gaia EDR3 and RVs from Gaia DR2. **We crossmatched this catalog with the catalog of distances inferred from Gaia EDR3 parallaxes (Bailer-Jones et al. 2021). We also crossmatched this catalog with the LAMOST DR5 catalog and the APOGEE DR16 stellar catalog (Cui et al. 2012; Ahumada et al. 2020; Xiang et al. 2019). We removed stars with angular separations larger than 150 milliarcseconds during each of these crossmatches. Stars with effective temperatures that differed by more than 500K between Gaia, APOGEE, and LAMOST were removed from the sample to minimize incorrect crossmatches. To remove stars with multiple crossmatches within 150 milliarcseconds, we only kept the star with the smallest angular separation. We also removed stars with a Gaia parallax < 0, parallax signal-to-noise ratio < 10, and Gaia astrometric excess noise > 5. To preferentially select single stars, we removed stars with `ruwe` ≥ 1.4, `ipd_frac_multi_peak` > 2, and `ipd_gof_harmonic_amplitude` ≥ 0.1.** After applying these cuts our total number of targets was 150,278. In total, 38,884 stars in our sample have at least one RV measurement from Gaia, LAMOST, or APOGEE; 23,013 have RVs from Gaia DR2, 22,420 from LAMOST DR5, and 7,697 from APOGEE DR16. The APOGEE survey (R = 22,500; Majewski et al. 2017) has a higher spectral resolution than Gaia (R = 11,500; Cropper et al. 2018), which in turn is higher than LAMOST (R = 1,800; Zhao et al. 2012). The median RV uncertainty for stars in our sample is around 0.1 km/s for APOGEE RVs, 1 km/s for Gaia RVS, and 5 km/s for LAMOST RVs. In cases where stars had two or more available RV measurements, we adopted APOGEE RVs as a first priority, followed by Gaia, then LAMOST.

Although RVs are available for more than one in three Kepler targets, most stars with RV measurements are bright. Very few of the faintest stars have RVs because of the selection functions of spectroscopic surveys. Most of the stars in our sample with Gaia RV measurements are brighter than around 14th magnitude in Gaia G-band, and stars with LAMOST or APOGEE RVs are mostly brighter than around 16th magnitude. Figure 1 shows the apparent magnitude distributions of the stars in our sample, with and without RVs. This figure reveals the combined selection functions of the Gaia, LAMOST and APOGEE RV surveys and shows that faint stars are less likely to have RV measurements than bright ones.

Figure 1. The distribution of apparent Gaia magnitudes for stars in our sample with and without RV measurements from Gaia, LAMOST and APOGEE.

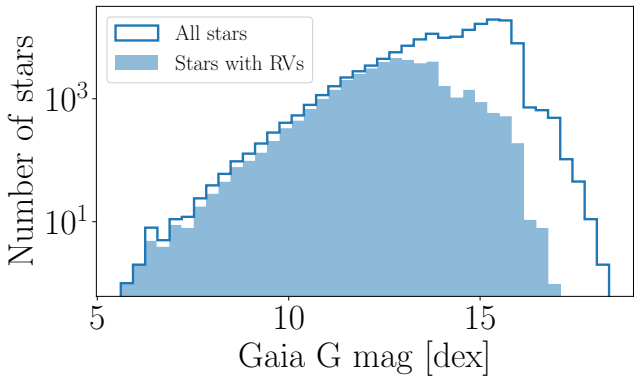

To illustrate how the populations of stars with and without RVs differ, we plot them on a color-magnitude diagram (CMD) in figure 2. The stars with RVs are generally hotter and more luminous than stars without. Most stars with RVs fall on the upper main sequence, the red giant branch, and the red clump. Most stars without RVs fall on the main sequence. This overall selection function is a combination of the APOGEE, LAMOST and Gaia DR2 selection functions.

In this paper, we construct a prior using stars with RV measurements which we then use to infer the velocities of stars without RV measurements. However, given that the populations of stars with and without RVs are so different, this could bias the velocities we infer, particularly if they are prior-dependent. We investigate this idea in section 3.2

and find that the $v_{\mathbf{x}}$ and $v_{\mathbf{z}}$ velocities we infer are relatively insensitive to the prior and therefore unlikely to biased, however the $v_{\mathbf{y}}$ velocities we infer should be used with caution as they are relatively prior-dependent.

Figure 2. A magnitude-temperature diagram of stars in the Kepler field with (left) and without (right) RVs provided by Gaia, LAMOST and APOGEE. The stars with RVs are generally hotter and more luminous than those without RVs, and include a large number of red clump stars and red giant branch stars. Stars without RVs are mostly concentrated on the main sequence.

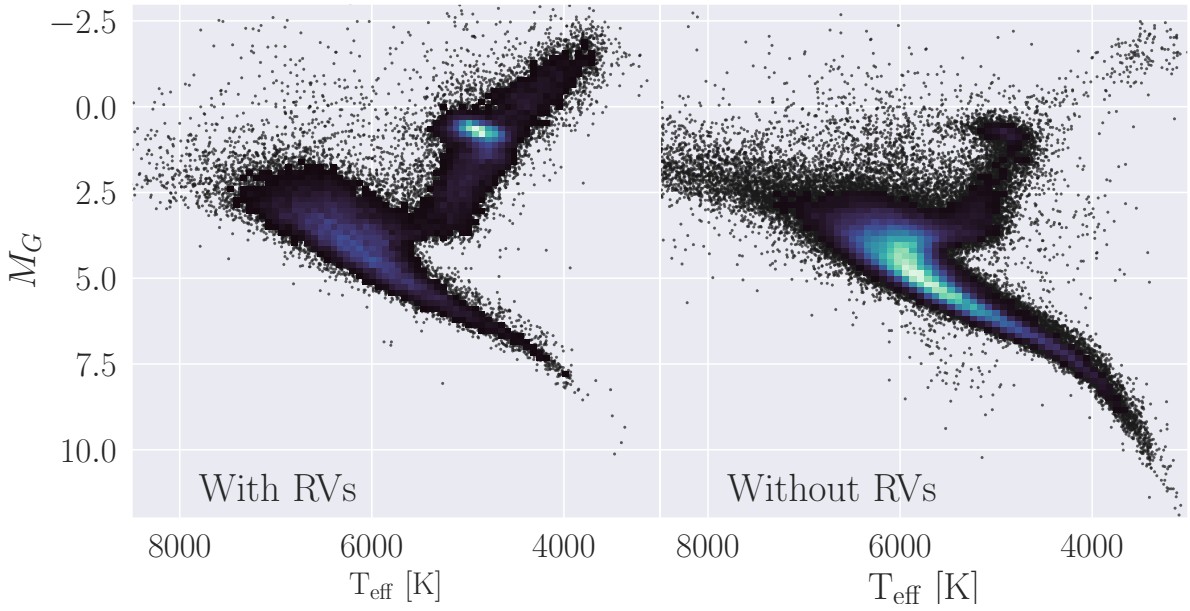

3. METHOD

In this section we describe how we calculate full 3D velocities for stars in the Kepler field. Around 1 in 3 Kepler targets have an RV from either Gaia, LAMOST, or APOGEE. For these 38,884 stars we calculated 3D velocities using the `coordinates` library of `astropy` (Astropy Collaboration et al. 2013; Price-Whelan et al. 2018). This library performs a series of matrix rotations and translations to convert stellar positions and velocities in equatorial coordinates into positions and velocities in Galactocentric coordinates. It converts positions, proper motions, parallaxes/distances, and RVs into $\mathbf{x}$, $\mathbf{y}$, $\mathbf{z}$, $v_{\mathbf{x}}$, $v_{\mathbf{y}}$, $v_{\mathbf{z}}$. For stars *without* RVs, we inferred their velocities by marginalizing over their RVs using the method described below.

3.1. *Inferring 3D velocities (marginalizing over missing RV measurements)*

For each star in our sample without an RV measurement, we inferred $v_{\mathbf{x}}$, $v_{\mathbf{y}}$, and $v_{\mathbf{z}}$ from the 3D positions – RA (α), dec (δ), and parallax (π), and 2D proper motions (μ_α and μ_δ) provided in the *Gaia* EDR3 catalog (Gaia Collaboration et al. 2020). We also simultaneously inferred distance (instead of using inverse-parallax) to model velocities (see *e.g.* Bailer-Jones 2015; Bailer-Jones et al. 2018).

Using Bayes rule, the posterior probability of the velocity parameters given the Gaia data can be written:

$$p(\mathbf{v_{xyz}}, D|\mu_\alpha, \mu_\delta, \alpha, \delta, \pi) = p(\mu_\alpha, \mu_\delta, \alpha, \delta, \pi|\mathbf{v_{xyz}}, D)p(\mathbf{v_{xyz}})p(D), \quad (1)$$

where D is distance and $\mathbf{v_{xyz}}$ is the 3D vector of velocities. To evaluate the likelihood function, our model predicts observable data from model parameters, *i.e.* it converts $v_{\mathbf{x}}$, $v_{\mathbf{y}}$ $v_{\mathbf{z}}$ and D to μ_α, μ_δ and π. In the first step of the model evaluation, cartesian coordinates, $\mathbf{x}$, $\mathbf{y}$, and $\mathbf{z}$ are calculated from α, δ, and D by applying a series of matrix rotations, and a translation to account for the Solar position. The cartesian Galactocentric velocity parameters, $v_{\mathbf{x}}$, $v_{\mathbf{y}}$, and $v_{\mathbf{z}}$, are then converted to equatorial coordinates, μ_α and μ_δ via another rotation. The posterior PDFs of the

parameters $v_{\mathbf{x}}$, $v_{\mathbf{y}}$, $v_{\mathbf{z}}$, and $\ln(D)$ are sampled by evaluating this model over a range of parameter values which are chosen by via the No U-Turns Sampler (NUTS) algorithm in `PyMC3`. At each set of model parameters the likelihood is calculated via a Gaussian likelihood function, and multiplied by a prior (described below) to produce the posterior probability: the probability of those model parameters given the data.

For computational efficiency, we used `PyMC3` to sample the posterior PDFs of stellar velocities (Salvatier et al. 2016). This required that we rewrite the `astropy` coordinate transformation code using `numpy` and `Theano` (Harris et al. 2020; The Theano Development Team et al. 2016). The series of rotations and translations required to convert from equatorial to Galactocentric coordinates is described in the astropy documentation[2] (Price-Whelan et al. 2018). For each star in the Kepler field, we explored the posteriors of the four parameters, $v_{\mathbf{x}}$, $v_{\mathbf{y}}$, $v_{\mathbf{z}}$, and $\ln(D)$ using the *PyMC3* No U-Turn Sampler (NUTS) algorithm, and the `exoplanet` *Python* library (Foreman-Mackey & Barentsen 2019). We tuned the *PyMC3* sampler for 1500 steps, with a target acceptance fraction of 0.9, then ran four chains of 1000 steps for a total of 4000 steps. This resulted in a $\hat{r}$-statistic (the ratio of intra-chain to inter-chain variance) of around unity, indicating convergence. Using PyMC3 made this inference procedure exceptionally fast – taking just a few seconds per star on a laptop.

3.2. *The prior*

As mentioned previously, the positioning of the Kepler field at low Galactic latitude allows $v_{\mathbf{z}}$ to be well-constrained from proper motion measurements alone. This also happens to be the case for $v_{\mathbf{x}}$, because the direction of the Kepler field is almost aligned with the **y**-axis of the Galactocentric coordinate system and is almost perpendicular to both the **x** and **z**-axes (see figure 3). For this reason, the **y**-direction is similar to the radial direction for observers near the Sun, so $v_{\mathbf{y}}$ will be poorly constrained for Kepler stars without RV measurements. On the other hand, $v_{\mathbf{x}}$ and $v_{\mathbf{z}}$ are almost perpendicular to the radial direction and can be precisely inferred with proper motions alone.

Figure 3. **x**, **y** and **z** positions of stars observed by Kepler, showing the orientation of the Kepler field. The Sun's position is indicated with a Solar symbol. The direction of the field is almost aligned with the **y**-axis and almost perpendicular to the **x** and **z**-axes, which is why $v_{\mathbf{x}}$ and $v_{\mathbf{z}}$ can be tightly constrained for Kepler stars without RVs, but $v_{\mathbf{y}}$ cannot.

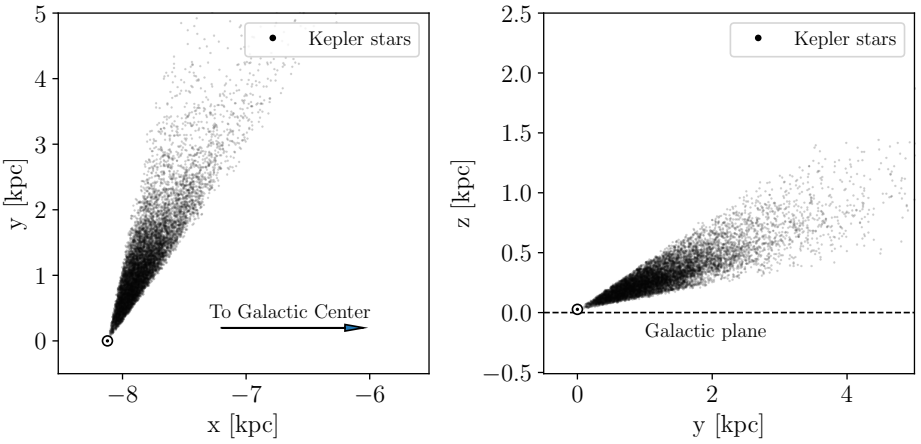

We constructed a multivariate Gaussian prior PDF over distance and 3D velocity using the Kepler targets *which have RV measurements*. We calculated the means and covariances of the $v_{\mathbf{x}}$, $v_{\mathbf{y}}$, $v_{\mathbf{z}}$ and $\ln(D)$ distributions of stars with measured RVs and then used these means and covariances to construct a multivariate Gaussian prior over the velocity and distance parameters for stars *without* RVs. Velocity and distance outliers greater than 3-σ were removed before calculating the means and covariances of the distributions. The distance and velocity distributions of Kepler targets with RVs are displayed in figure 4. These are the distributions we used to construct the prior. The 1- and 2-σ contours of the multivariate Gaussian prior is shown in each panel in red. **This figure shows that Gaussian functions only approximately reproduce the true velocity distributions. We could have chosen a more complex prior that would fit these data better, however since this prior is constructed using stars with**

[2] https://docs.astropy.org/en/stable/coordinates/galactocentric.html

RVs, which may have a slightly different velocity distribution to stars without RVs, we opted for the more uninformative, simple Gaussian prior.

Figure 4. The velocity and distance distributions for stars with RV measurements, used to construct a multivariate Gaussian prior over velocity and distance parameters for stars *without* RVs. The 1- and 2-D distributions of the data are shown in black and the prior is indicated in red.

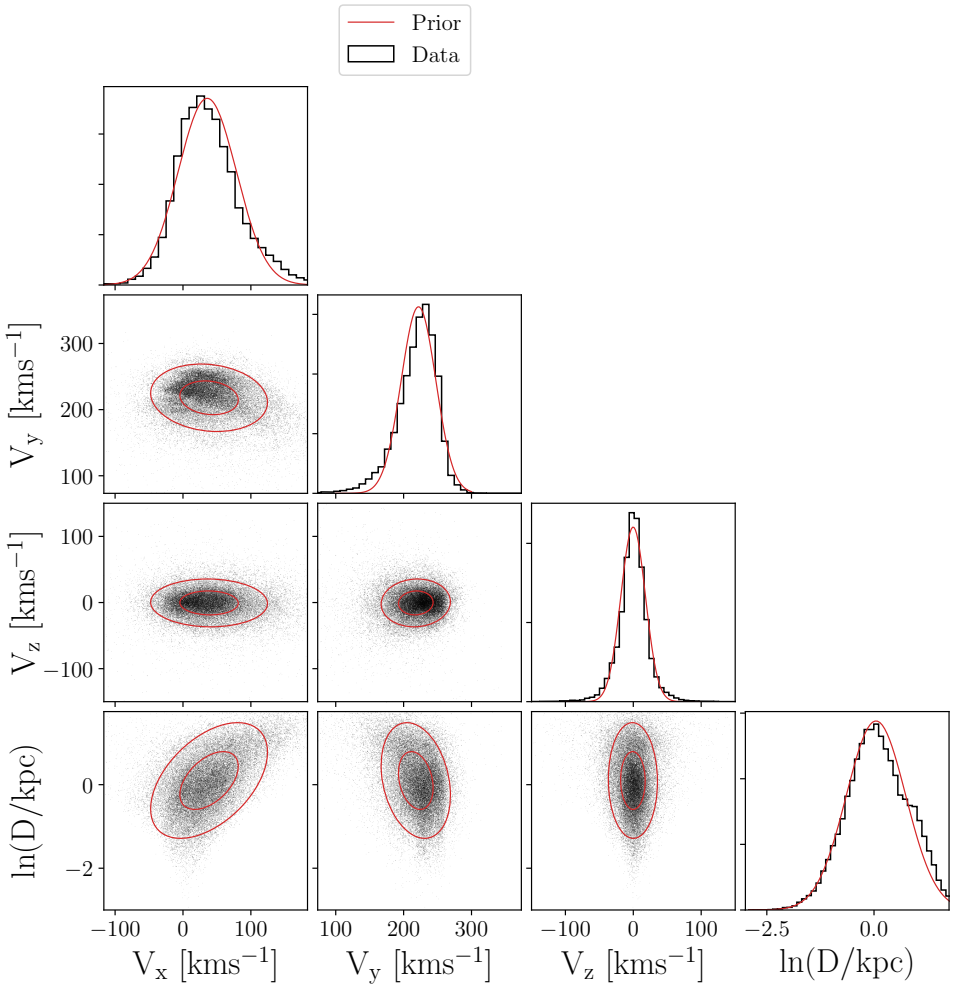

Our goal was to infer the velocities of stars *without* RV measurements using a prior calculated from stars *with* RV measurements. However, stars with and without RVs are likely to be quite different populations, determined by the Gaia, LAMOST and APOGEE selection functions. In particular, stars without RV measurements are more likely to be fainter, less luminous, cooler and potentially older. Figure 2 shows the populations of stars with and without RVs on the CMD – stars with RVs are more likely to be upper-main-sequence and red giant stars, and stars without RVs are more likely to be mid and lower main-sequence dwarfs. For this reason, a prior based on the velocity distributions of stars *with* RVs will not necessarily reflect the velocities of those without. **We could have opted to construct a prior that depends on CMD position, however, in practice, this would require making a number of arbitrary choices, so we instead opted for a simpler approach. In addition, we find that the $v_{\mathbf{x}}$ and $v_{\mathbf{z}}$ velocities we infer are not strongly influenced by the prior, as described below.**

We tested the influence of the prior on the velocities we inferred. One of the main features of the RV selection functions is brightness: Gaia DR2 RVs are only available for stars brighter than around 14th magnitude, and LAMOST

DR5 and APOGEE DR16 RVs for stars brighter than around 16th magnitude. For this reason, we tested priors based on stellar populations with different apparent magnitudes. Three priors were tested: one calculated from the velocity distributions of the brightest half of the RV sample (*Gaia* G-band apparent magnitude < 13), one from the faintest half ($G > 13$), and one from *all* stars with RVs. Figure 5 shows the distributions of the faint (blue) and bright (orange) halves of the RV sample as kernel density estimates (KDEs). The distributions are different because bright stars are typically more massive, younger, more evolved, and/or closer to the Sun on average than faint stars. As a result, these stars occupy slightly different Galactic orbits. The multivariate Gaussian, fit to these distributions, which was used as a prior PDF, is shown as single-dimension projections in figure 5. The Gaussian fit to the bright and faint star distributions are shown as dashed orange and blue lines, respectively. The Gaussian fit to *all* the data, both bright and faint, is shown as a black solid line. The means of the faint and bright distributions differ by 6 kms^{-1}, 5 kms^{-1}, 1 kms^{-1} and 0.21 kpc, for $v_{\mathbf{x}}$ $v_{\mathbf{y}}$, $v_{\mathbf{z}}$ and $\ln(D)$, respectively. The $v_{\mathbf{x}}$, $v_{\mathbf{y}}$, and distance distributions of the bright stars are slightly non-Gaussian – more so than the faint stars. This highlights the inadequacy of using a Gaussian distribution as the prior – a Gaussian is only an approximation of the underlying distribution of stars in our sample. As a result of this approximation, inferred velocities that are strongly prior-dependent – (*i.e.* especially those in the **y**-direction) may inherit some inaccuracies from the Gaussian prior, which is not a perfect representation of the underlying data. However, given that the populations of stars with and without RV measurements are different, it may be inappropriate to use a more complex, more informative prior anyway.

Figure 5. Velocity and distance distributions of faint (blue) and bright (orange) stars with RVs, shown as KDEs. Gaussian fits to these distributions are shown as dashed lines in corresponding colors. The solid black line shows the Gaussian fit to all data (bright and faint combined) and is the prior we ended up using in our model.

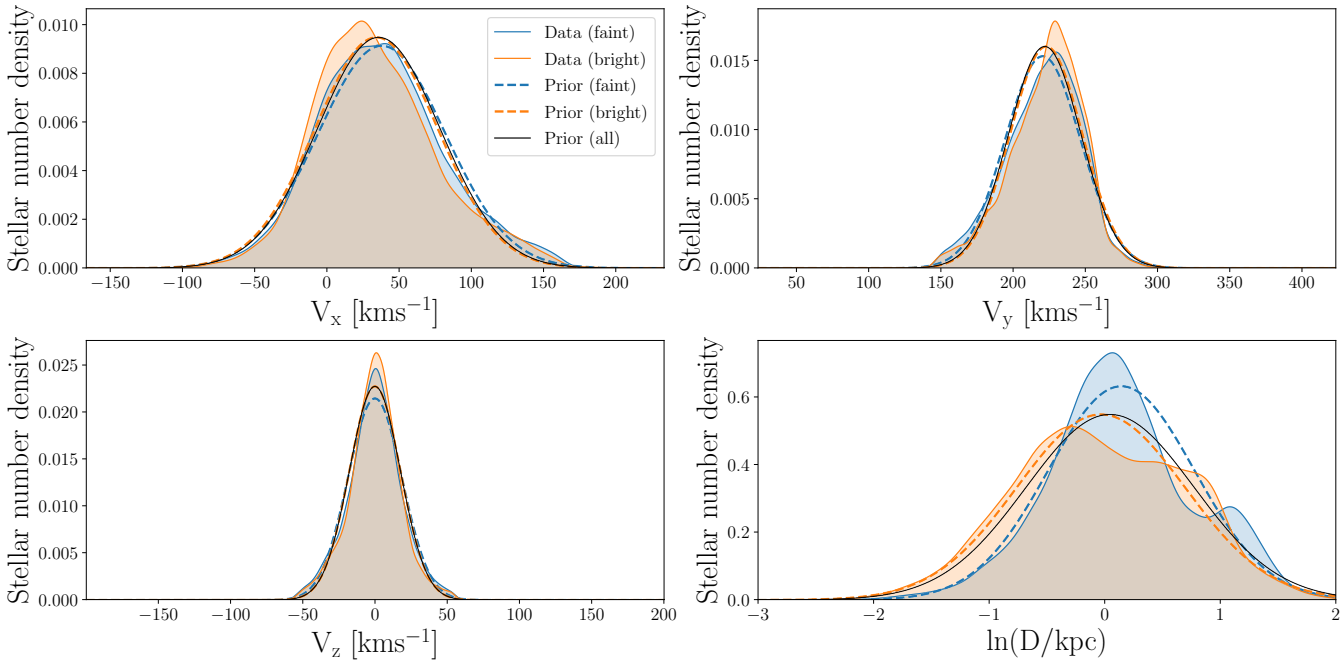

We inferred the velocities of 1000 stars chosen at random from the RV Kepler sample using each of these three priors and compared the inferred velocity distributions. If the inferred velocities were highly prior-dependent, the resulting distributions, obtained from different priors, would look very different. The results of this test are shown in figure 6. From left to right, the three panels show the distributions of inferred $v_{\mathbf{x}}$, $v_{\mathbf{y}}$, and $v_{\mathbf{z}}$. The blue dashed line shows a KDE, representing the distributions of velocities inferred using the prior calculated from the faint half of the RV sample. Similarly, the solid orange line shows the distribution of inferred velocities using the prior calculated from the bright half of the RV sample, and the solid black line shows the results of the prior calculated from *all* stars with measured RVs.

The median values of the $v_{\mathbf{y}}$ distributions resulting from the faint and bright priors differ by around 4 kms^{-1}. This is similar to the difference in means of the faint and bright populations (5 kms^{-1}, as quoted above). The inferred $v_{\mathbf{x}}$ and $v_{\mathbf{z}}$ distributions differ by 2 kms^{-1} and 0.3 kms^{-1}, respectively. Regardless of the prior choice, the $v_{\mathbf{x}}$ and $v_{\mathbf{z}}$ distributions are similar because velocities in the **x** and **z**-directions are not strongly prior dependent: they are tightly constrained with proper motion measurements alone. However, the distribution of inferred $v_{\mathbf{y}}$ velocities *does* depend on the prior. This is because the **y**-direction is close to the radial direction for Kepler stars (see figure 3), and $v_{\mathbf{y}}$ cannot be tightly constrained without an RV measurement. The distributions of stellar distances are almost identical, irrespective of the prior. This is because distance is very tightly constrained by Gaia parallax and is relatively insensitive to the prior.

Figure 6. The distributions of velocity and distance parameters, inferred using three different priors. The orange line is a KDE that represents the distribution of parameters inferred with a Gaussian prior, estimated from the bright half of the RV sample ($G < 13$). The blue dashed line shows the results from a prior estimated from the faint half of the RV sample ($G > 13$)). The black line shows the results from a prior calculated from all stars with RV measurements and is the prior we adopt in our final analysis.

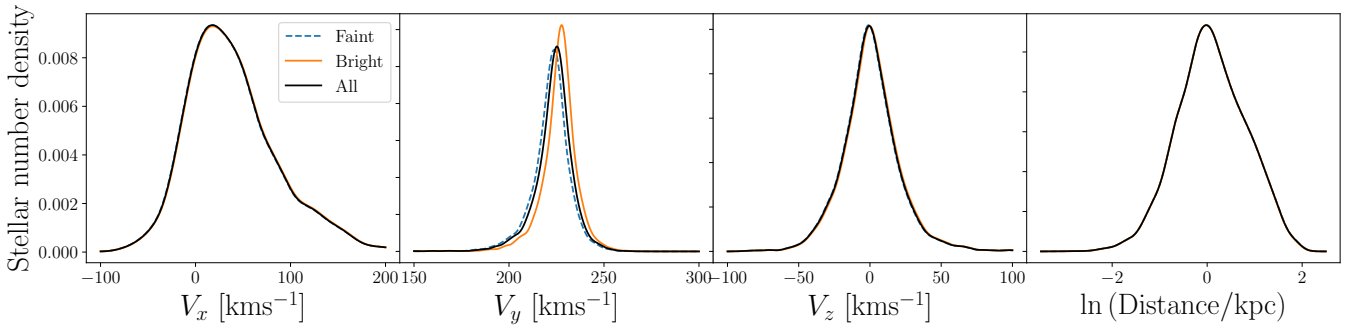

Although this test was performed on stars with RV measurements, which are brighter overall than the sample of stars without RVs (*e.g.* figure 1), figure 6 nevertheless shows that $v_{\mathbf{x}}$ and $v_{\mathbf{z}}$ are not strongly prior-dependent. Since this work is chiefly motivated by kinematic age-dating, which mostly requires vertical velocities ($v_{\mathbf{z}}$) we are satisfied with these results. The difference in the dispersions of $v_{\mathbf{z}}$ velocities, calculated with the three different priors tested above was smaller than 0.5 kms^{-1}. We conclude that the $v_{\mathbf{x}}$ and $v_{\mathbf{z}}$ velocities we infer are relatively insensitive to prior choice, and we adopt a prior calculated from the distributions of all stars with RV measurements (black Gaussians in figure 5). The $v_{\mathbf{y}}$ velocities are more strongly prior dependent and should be used with caution.

Figure 7 shows the posterior PDF over velocity and distance parameters for a randomly selected Kepler target with an RV measurement, KIC 12218729. Blue lines in each panel indicate the velocities calculated using the RV measurement and the distributions indicated the probability density of the parameters, inferred *without* the RV measurement. The velocity parameters are correlated because the lack of RV introduces a slight degeneracy: the star's proper motion can be equally well described with a range of different velocities. The star's posterior PDF is particularly elongated in $v_{\mathbf{y}}$, which is the velocity most similar to RV. The star's distance is not tightly correlated with its velocity parameters because it is precisely determined by parallax.

4. RESULTS

4.1. *Inferred velocities*

In this section we assess the quality of the 3D stellar velocities we infer. Figure 8 shows the distribution of stellar velocities inferred for 5000 randomly selected Kepler stars. The 2D distributions of inferred stellar velocities are plotted in the lower-left panels, with black contours indicating the stellar number density. The red contours in these panels show the marginal projections of the Gaussian prior in 2D. The diagonal panels show the 1D distributions (histograms) of stellar velocities. The black histogram shows the distribution of inferred velocities, the cyan histogram shows the distribution of velocities calculated for stars with RVs (on which the prior was based), and the red lines show the 1D prior distributions. The prior distribution is calculated using the velocities of stars with RVs. If the velocity distributions of stars were Gaussian, the 1D red Gaussians would look like the cyan histograms. In other words, the

Figure 7. The posterior PDF over parameters $v_{\mathbf{x}}$, $v_{\mathbf{y}}$, $v_{\mathbf{z}}$ and ln(distance) for a Kepler target chosen at random: KIC 12218729. This figure shows that the velocity parameters are correlated and the star's posterior is elongated in $v_{\mathbf{y}}$.

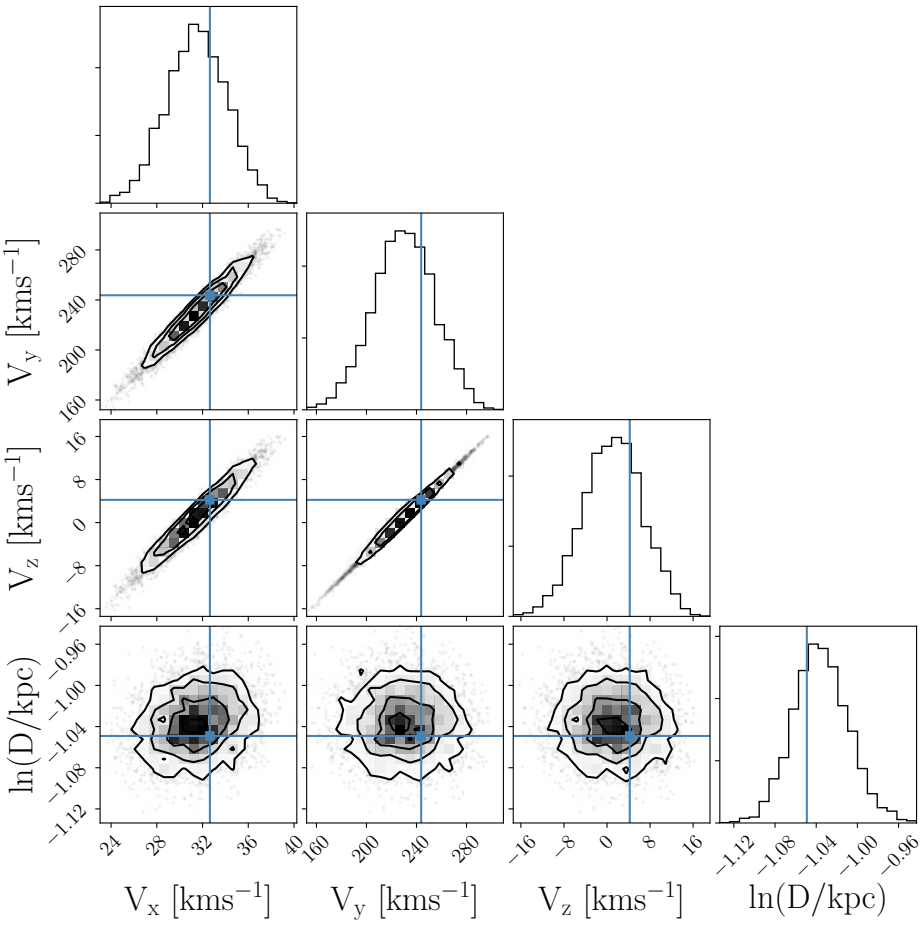

differences between the red lines and cyan histograms is caused by the non-Gaussianity of the velocity distributions. In each panel, the distribution of inferred velocities is similar to the distribution of directly-measured velocities; the velocities of stars calculated with and without RVs are broadly similar.

There is a slight negative correlation between inferred $v_{\mathbf{y}}$ and $v_{\mathbf{z}}$ velocities, which is visible in the central panel of figure 8. This negative correlation is not seen in the prior, nor is it apparent in the posteriors of individual stars: figure 7 shows that the $v_{\mathbf{y}}$ and $v_{\mathbf{z}}$ parameters are *positively* correlated for KIC 12218729. The negative correlation seen in the population of inferred velocities is caused by the specific orientation of the Kepler field which creates a slight degeneracy between $v_{\mathbf{y}}$ and $v_{\mathbf{z}}$. This orientation creates a negative correlation in the population of stars, that is not apparent in the posteriors of individual stars. To an observer looking at Kepler field, a star with either a positive $v_{\mathbf{z}}$ or a *negative* $v_{\mathbf{y}}$ would appear to move in the direction of positive $v_{\mathbf{z}}$, when projected onto the sky. In this sense, $v_{\mathbf{y}}$ and $v_{\mathbf{z}}$ are negatively correlated. However, the observed proper motions of a star without a measured RV could be equally well described by either increasing both $v_{\mathbf{y}}$ and $v_{\mathbf{z}}$, or decreasing both $v_{\mathbf{y}}$ and $v_{\mathbf{z}}$. For this reason, the star's posterior PDF over $v_{\mathbf{y}}$ and $v_{\mathbf{z}}$ will be positively correlated. This results in a paradox that is similar to Simpson's paradox: the posteriors over vy and vz are positively correlated for individual stars, however the vy and vz velocities of the population are negatively correlated.

To further validate our method, we compare inferred velocities with directly-calculated velocities for stars in our sample with measured RVs. Figure 9 shows the $v_{\mathbf{x}}$, $v_{\mathbf{y}}$ and $v_{\mathbf{z}}$ velocities, and distances we inferred, compared with those calculated from measured RVs, for 5000 Kepler stars chosen at random. The three velocity components, $v_{\mathbf{x}}$, $v_{\mathbf{y}}$ and $v_{\mathbf{z}}$ were recovered with differing levels of precision: $v_{\mathbf{x}}$ and $v_{\mathbf{z}}$ are inferred more precisely than $v_{\mathbf{y}}$. This is because of the position of the Kepler field, shown in figure 3. The velocities of low-$v_{\mathbf{y}}$ stars are overestimated and the velocities of

Figure 8. The distribution of inferred stellar velocities and distances. Figure 8 shows the inferred velocities of 5000 randomly selected Kepler stars. The 2D distributions of inferred stellar velocities are plotted in the lower-left panels, with black contours indicating the stellar number density. The red contours in the lower-left panels show the marginal projections of the Gaussian prior distribution in 2D. The upper-right panels in the figure, lying on the plot's diagonal, show the 1D distributions (histograms) of stellar velocities. The black histogram shows the distribution of inferred velocities, the blue histogram shows the distribution of velocities for stars with RVs, and the red lines show the 1D marginal Gaussian prior distributions.

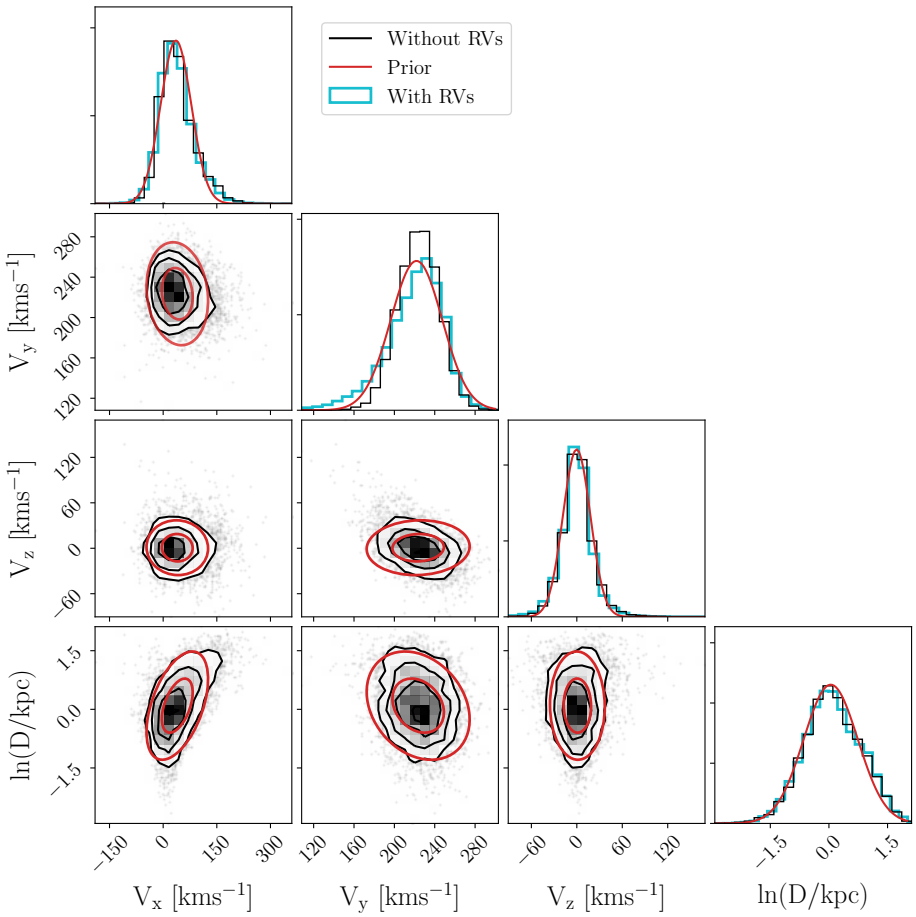

high-$v_{\mathbf{y}}$ stars are underestimated. This is because there is little information to constrain the $v_{\mathbf{y}}$ velocities and the prior pulls the $v_{\mathbf{y}}$ velocities toward the center of the distribution. The $v_{\mathbf{x}}$, $v_{\mathbf{y}}$ and $v_{\mathbf{z}}$ velocities of stars are correlated, which means that stars with an inaccurate $v_{\mathbf{y}}$ also have slightly accurate $v_{\mathbf{z}}$ and $v_{\mathbf{x}}$. Despite slight systematic inaccuracies **visible in the residual (bottom) panels of figure 9**, around 68% of the inferred velocities are within 1σ of their true velocities; the inferred velocities are consistent with the true velocities.

We provide a table of the directly-calculated, and indirectly-inferred 3D velocities of stars observed by Kepler, in addition to their positional and velocity information from Gaia EDR3, LAMOST DR5 and APOGEE DR16. A description of each column included in that table is provided in table 1.

5. CONCLUSION

This paper describes a method for inferring the 3D velocities of stars by marginalizing over missing radial velocity measurements. We focused on stars in the Kepler field because of its potential for studying stellar evolution via kinematic age-dating as well as its advantageous orientation. Located at low Galactic latitude, the Kepler field is almost aligned with the y-axis of the Galactocentric coordinate system. This means that 2D Gaia proper motion measurements alone are sufficient to tightly constrain the $v_{\mathbf{x}}$ and $v_{\mathbf{z}}$ velocities of Kepler stars. Without RV measurements, the $v_{\mathbf{y}}$ velocities of Kepler stars are poorly constrained. However, given that many age-velocity dispersion relations (AVR)

Figure 9. Velocities calculated with full 6D information compared with velocities inferred without RVs, for 5000 Kepler targets with RV measurements.

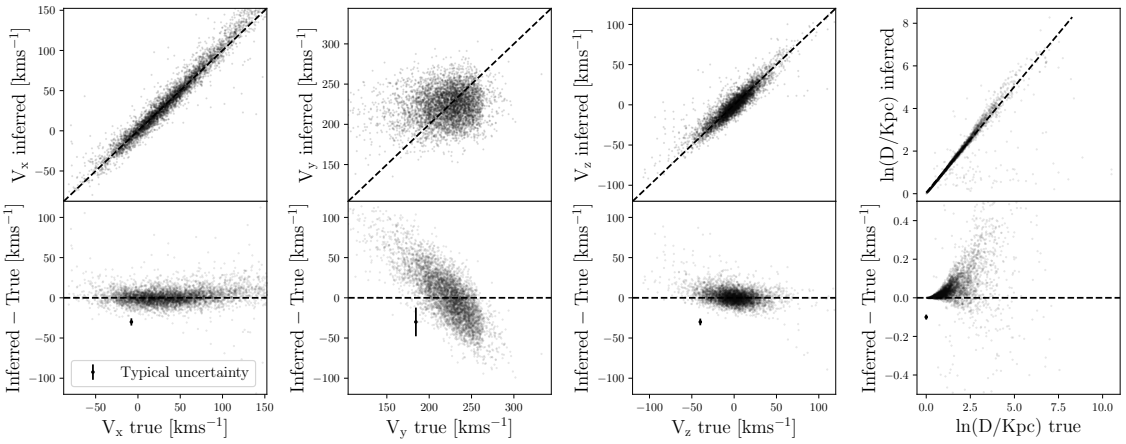

Table 1. The list of columns in the data table published online, which provides the velocities and kinematic information for stars in the Kepler field.

Column name	Description
`kic_id`	The Kepler Input Catalog ID number of the target.
`source_id`	The Gaia DR3 ID number of the target.
`ra, ra_error`	Gaia EDR3 right ascenscion (°).
`dec, dec_error`	Gaia EDR3 declination in degrees (°).
`parallax, parallax_error`	Gaia EDR3 parallax (mas).
`r_est, r_est_err`	Distance (parsec), provided by Bailer-Jones et al. (2021).
`pmra, pmra_error`	Gaia EDR3 proper motion in right ascension (mas/yr).
`pmdec, pmdec_error`	Gaia EDR3 proper motion in declination (mas/yr).
`gaia_rv, gaia_rv_error`	Gaia DR2 radial velocity (km/s)
`apogee_rv, apogee_rv_error`	APOGEE DR16 radial velocity (km/s)
`lamost_rv, lamost_rv_error`	LAMOST DR5 radial velocity (km/s)
`vx_calc`	The $v_{\mathbf{x}}$ velocity calculated using RV (km/s).
`vx_inferred, vx_inferred_error`	The median and standard deviation of $v_{\mathbf{x}}$ velocity samples, inferred without RV (km/s).
`vy_calc`	The $v_{\mathbf{y}}$ velocity calculated using RV (km/s).
`vy_inferred, vy_inferred_error`	The median and standard deviation of $v_{\mathbf{y}}$ velocity samples, inferred without RV (km/s).
`vz_calc`	The $v_{\mathbf{z}}$ velocity calculated using RV (km/s).
`vz_inferred, vz_inferred_error`	The median and standard deviation of $v_{\mathbf{z}}$ velocity samples, inferred without RV (km/s).
`vxvy_covar`	The covariance between $v_{\mathbf{x}}$ and $v_{\mathbf{y}}$ samples.
`vxvz_covar`	The covariance between $v_{\mathbf{x}}$ and $v_{\mathbf{z}}$ samples.
`vxlnd_covar`	The covariance between $v_{\mathbf{x}}$ and ln(distance) samples.
`vyvz_covar`	The covariance between $v_{\mathbf{y}}$ and $v_{\mathbf{z}}$ samples.
`vylnd_covar`	The covariance between $v_{\mathbf{y}}$ and ln(distance) samples.
`vzlnd_covar`	The covariance between $v_{\mathbf{z}}$ and ln(distance) samples.

are calibrated in *vertical* velocity, $v_{\mathbf{z}}$ is the main parameter of interest for kinematic age-dating and it is precisely constrained by our method: $v_{\mathbf{z}}$ is inferred with a median precision of 4 kms^{-1}.

We compiled kinematic data for Kepler targets from the, Gaia EDR3, LAMOST DR5 and APOGEE DR16 catalogs. Gaia EDR3 provided parallaxes, positions and proper motions for the stars in our sample. Altogether, Gaia DR2, LAMOST DR5, and APOGEE DR16 provided RVs for 38,884 Kepler targets.

We calculated $v_{\mathbf{x}}$, $v_{\mathbf{y}}$, and $v_{\mathbf{z}}$ for the 38,884 stars in our sample with RVs using `astropy`. For the remaining stars, we *inferred* $v_{\mathbf{x}}$, $v_{\mathbf{y}}$, $v_{\mathbf{z}}$, and distance while marginalizing over RV. Our prior was a 4D Gaussian in $v_{\mathbf{x}}$, $v_{\mathbf{y}}$, $v_{\mathbf{z}}$ and ln(distance), which was based on the distribution of stars in our sample *with* RVs. Since the populations of stars with and without RVs in the Kepler field are somewhat different – stars *with* RVs are generally brighter than stars without – we tested the sensitivity of our results to the prior. We split the subsample of stars with measured RVs into two further subgroups: stars brighter and stars fainter than 13th magnitude in Gaia G-band (13th being the median magnitude of the Kepler stars with RVs). Priors were constructed from the faint and bright halves of the sample and used to infer the velocities of 1000 stars randomly selected from the total RV sample. Upon examination, we found the final inferred velocities were similar, irrespective of the prior. As expected, $v_{\mathbf{x}}$ and $v_{\mathbf{z}}$ depend very little on the prior but $v_{\mathbf{y}}$ has a stronger prior-dependence because it is difficult to constrain without an RV for Kepler stars. A caveat of our inferred velocities is therefore that the $v_{\mathbf{y}}$ velocities may not be accurate for faint stars in the Kepler field. The median precision of inferred $v_{\mathbf{x}}$, $v_{\mathbf{y}}$, and $v_{\mathbf{z}}$ velocities is 5, 18, and 4 kms^{-1} respectively. We provide a table of parameters $v_{\mathbf{x}}$, $v_{\mathbf{y}}$, $v_{\mathbf{z}}$, and ln(distance), with uncertainties and covariances, for a total of 150,278 Kepler targets. This table also contains the positional and velocity information from Gaia DR2, Gaia EDR3, LAMOST DR5, and APOGEE DR16 used in this project.

ACKNOWLEDGEMENTS

RA acknowledges support from Astrophysics Data Analysis Program award ADAP #80NSSC21K0636.

JCZ is supported by an NSF Astronomy and Astrophysics Postdoctoral Fellowship under award AST-2001869.

This work made use of the gaia-kepler.fun crossmatch database created by Megan Bedell.

Some of the data presented in this paper were obtained from the Mikulski Archive for Space Telescopes (MAST). STScI is operated by the Association of Universities for Research in Astronomy, Inc., under NASA contract NAS5-26555. Support for MAST for non-HST data is provided by the NASA Office of Space Science via grant NNX09AF08G and by other grants and contracts. This paper includes data collected by the Kepler mission. Funding for the Kepler mission is provided by the NASA Science Mission directorate.

This work has made use of data from the European Space Agency (ESA) mission *Gaia* (https://www.cosmos.esa.int/gaia), processed by the *Gaia* Data Processing and Analysis Consortium (DPAC, https://www.cosmos.esa.int/web/gaia/dpac/consortium). Funding for the DPAC has been provided by national institutions, in particular the institutions participating in the *Gaia* Multilateral Agreement.

Software: Astropy (**?**), Matplotlib (**?**), Seaborn, etc

REFERENCES

Ahumada, R., Prieto, C. A., Almeida, A., & *et al.* 2020, ApJS, 249, 3, doi: 10.3847/1538-4365/ab929e

Angus, R., Aigrain, S., & Foreman-Mackey *et al*, D. 2015, MNRAS, 450, 1787, doi: 10.1093/mnras/stv423

Angus, R., Morton, T. D., & Foreman-Mackey *et al*, D. 2019, AJ, 158, 173, doi: 10.3847/1538-3881/ab3c53

Angus, R., Beane, A., Price-Whelan, A. M., et al. 2020, AJ, 160, 90, doi: 10.3847/1538-3881/ab91b2

Astropy Collaboration, Robitaille, T. P., & Tollerud *et al*, E. J. 2013, A&A, 558, A33, doi: 10.1051/0004-6361/201322068

Aumer, M., & Binney, J. J. 2009, MNRAS, 397, 1286, doi: 10.1111/j.1365-2966.2009.15053.x

Bailer-Jones, C. A. L. 2015, PASP, 127, 994, doi: 10.1086/683116

Bailer-Jones, C. A. L., Rybizki, J., Fouesneau, M., Demleitner, M., & Andrae, R. 2021, AJ, 161, 147, doi: 10.3847/1538-3881/abd806

Bailer-Jones, C. A. L., Rybizki, J., & Fouesneau *et al*, M. 2018, AJ, 156, 58, doi: 10.3847/1538-3881/aacb21

Barnes, S. A. 2003, ApJ, 586, 464, doi: 10.1086/367639

—. 2007, ApJ, 669, 1167, doi: 10.1086/519295

Casagrande, L., Schönrich, R., & Asplund *et al*, M. 2011, A&A, 530, A138, doi: 10.1051/0004-6361/201016276

Claytor, Z. R., van Saders, J. L., Santos, Â. R. G., et al. 2020, ApJ, 888, 43, doi: 10.3847/1538-4357/ab5c24

Cropper, M., Katz, D., Sartoretti, P., et al. 2018, A&A, 616, A5, doi: 10.1051/0004-6361/201832763

Cui, X.-Q., Zhao, Y.-H., & Chu *et al.*, Y.-Q. 2012, Research in Astronomy and Astrophysics, 12, 1197, doi: 10.1088/1674-4527/12/9/003

Curtis, J. L., Agüeros, M. A., Matt, S. P., et al. 2020, ApJ, 904, 140, doi: 10.3847/1538-4357/abbf58

Dropulic, A., Ostdiek, B., Chang, L. J., et al. 2021, arXiv e-prints, arXiv:2103.14039. https://arxiv.org/abs/2103.14039

Foreman-Mackey, D., & Barentsen, G. 2019, dfm/exoplanet: exoplanet v0.1.3, v0.1.3, Zenodo, doi: 10.5281/zenodo.2536576

Gaia Collaboration, Brown, A. G. A., Vallenari, A., et al. 2020, arXiv e-prints, arXiv:2012.01533. https://arxiv.org/abs/2012.01533

Gaia Collaboration, Brown, A. G. A., Vallenari, A., & Prusti, T. *et al.* 2018, A&A, 616, A1, doi: 10.1051/0004-6361/201833051

Gaia Collaboration, Prusti, T., de Bruijne, J. H. J., & Brown, A. G. A. *et al.*. 2016, A&A, 595, A1, doi: 10.1051/0004-6361/201629272

Harris, C. R., Millman, K. J., van der Walt, S. J., et al. 2020, Nature, 585, 357, doi: 10.1038/s41586-020-2649-2

Holmberg, J., Nordström, B., & Andersen, J. 2007, A&A, 475, 519, doi: 10.1051/0004-6361:20077221

—. 2009, A&A, 501, 941, doi: 10.1051/0004-6361/200811191

Lindegren, L., & Dravins, D. 2021, A&A, 652, A45, doi: 10.1051/0004-6361/202141344

Lu, Yuxi, Angus, R., et al. 2021, arXiv e-prints, arXiv:2102.01772. https://arxiv.org/abs/2102.01772

Mackereth, J. T., Bovy, J., Leung, H. W., et al. 2019, MNRAS, 489, 176, doi: 10.1093/mnras/stz1521

Majewski, S. R., Schiavon, R. P., Frinchaboy, P. M., et al. 2017, AJ, 154, 94, doi: 10.3847/1538-3881/aa784d

Mamajek, E. E., & Hillenbrand, L. A. 2008, ApJ, 687, 1264, doi: 10.1086/591785

Matt, S. P., MacGregor, K. B., & Pinsonneault *et al*, M. H. 2012, ApJL, 754, L26, doi: 10.1088/2041-8205/754/2/L26

Metcalfe, T. S., & Egeland, R. 2019, ApJ, 871, 39, doi: 10.3847/1538-4357/aaf575

Nordström, B., Mayor, M., & Andersen *et al*, J. 2004, A&A, 418, 989, doi: 10.1051/0004-6361:20035959

Oh, S., Price-Whelan, A. M., Hogg, D. W., Morton, T. D., & Spergel, D. N. 2017, AJ, 153, 257, doi: 10.3847/1538-3881/aa6ffd

Price-Whelan, A. M., Sipőcz, B. M., & Günther *et al*, H. M. 2018, AJ, 156, 123, doi: 10.3847/1538-3881/aabc4f

Salvatier, J., Wiecki, T. V., & Fonnesbeck, C. 2016, PyMC3: Python probabilistic programming framework. http://ascl.net/1610.016

Skumanich, A. 1972, ApJ, 171, 565, doi: 10.1086/151310

Soderblom, D. R. 2010, ARA&A, 48, 581, doi: 10.1146/annurev-astro-081309-130806

Spada, F., & Lanzafame, A. C. 2019, arXiv e-prints, arXiv:1908.00345. https://arxiv.org/abs/1908.00345

Strömberg, G. 1946, ApJ, 104, 12, doi: 10.1086/144830

The Theano Development Team, Al-Rfou, R., Alain, G., et al. 2016, arXiv e-prints, arXiv:1605.02688. https://arxiv.org/abs/1605.02688

Ting, Y.-S., & Rix, H.-W. 2019, ApJ, 878, 21, doi: 10.3847/1538-4357/ab1ea5

van Saders, J. L., Ceillier, T., & Metcalfe *et al*, T. S. 2016, Nature, 529, 181, doi: 10.1038/nature16168

van Saders, J. L., Pinsonneault, M. H., & Barbieri, M. 2018, ArXiv e-prints. https://arxiv.org/abs/1803.04971

Wielen, R. 1977, A&A, 60, 263

Xiang, M., Ting, Y.-S., & Rix *et al.*, H.-W. 2019, ApJS, 245, 34, doi: 10.3847/1538-4365/ab5364

Yu, J., & Liu, C. 2018, MNRAS, 475, 1093, doi: 10.1093/mnras/stx3204

Zhao, G., Zhao, Y.-H., Chu, Y.-Q., Jing, Y.-P., & Deng, L.-C. 2012, Research in Astronomy and Astrophysics, 12, 723, doi: 10.1088/1674-4527/12/7/002